Advanced Control Strategy of Back-to-Back PWM Converters in PMSG Wind Power System

Tan Luong VAN[1], *Thanh Dung NGUYEN*[2], *Thanh Trang TRAN*[2,3], *Huy Dung NGUYEN*[4]

[1]Faculty of Electronics and Telecommunications, Sai Gon University, 273 An Duong Vuong, Ho Chi Minh City, Vietnam
[2]Faculty of Engineering and Technology, Van Hien University, 665-667-669 Dien Bien Phu, Ho Chi Minh City, Vietnam
[3]National Key Lab of Digital Control and System Engineering, Ho Chi Minh City University of Technology, 268 Ly Thuong Kiet, Ho Chi Minh City, Vietnam
[4]Faculty of Electronics and Automatic Control Engineering, Ho Chi Minh City Electric Power College, 554 Ha Huy Giap, Ho Chi Minh City, Vietnam

luongees2@yahoo.com, thanhdungcatc@gmail.com, trangtt@vhu.edu.vn, trangtranthanh1979@gmail.com, dungthd2@yahoo.com

DOI: 10.15598/aeee.v13i2.1161

Abstract. *This paper proposes a control scheme of back-to-back PWM converters for the permanent magnet synchronous generator (PMSG) wind turbine system. The DC-link voltage can be controlled at the machine-side converter (MSC), while the grid-side converter (GSC) controls the grid active power for a maximum power point tracking (MPPT). At the grid fault condition, the DC-link voltage controller is designed using a feedback linearization (FL) theory. For the MPPT, a proportional control loop is added to the torque control to reduce the influence of the inertia moment in the wind turbines, which can improve its dynamic performance. The validity of this control algorithm has been verified by the simulation of the 2-MW PMSG wind turbine system.*

Keywords

DC-link voltage, feedback linearization, MPPT, PMSG, sag, swell.

1. Introduction

In the recent years, the wind power generation has been concerned as one of the most rapidly growing energy sources in the world since the natural resources are becoming exhausted. In the variable-speed wind turbine (WT) systems, a direct-drive wind energy conversion system based on PMSGs has a lot of advantages such as no gearbox, high precision, high power density, and simple control method, except initial installation costs [1], [2].

As the scale of wind farms becomes larger and larger, the condition of the grid-connected wind turbines is more important. Recently, some countries have issued the dedicated grid codes for connecting the wind turbine system to the grid [3], [4]. Also, the smart-grid and the micro-grid have been researched for the efficiency of the power management [5], [6]. However, the grid voltage in these systems is more fluctuated than that of the conventional grid. Therefore, an advanced control of the wind power generation system is required for the grid abnormal conditions.

Several solutions have been proposed for the grid faults in the variable-speed wind turbine systems. For the low voltage ride-through (LVRT) purpose, a crowbar system consisting an external resistor is connected in the rotor-side of the doubly-fed induction generator (DFIG) to absorb the active power during the grid fault [7], [8]. The wind turbine keeps operating to produce the active power, whereas the reactive power or the voltage at the grid connection is controlled by the GSC. Nevertheless, during a grid fault and in the case of a weak grid, the GSC cannot provide sufficient reactive power or voltage support due to its small power capacity and there is a risk of voltage instability. Also, to guarantee the uninterrupted operation of a DFIG wind turbine during the grid faults, a static synchronous compensator (STATCOM) which is installed at the point of common coupling (PCC) has been used

to inject the reactive power to the grid [9], [10], [11]. However, it is not used alone for the DFIG ride-through capability since it cannot protect the rotor-side converter (RSC) during a grid fault. On the other words, it should be used in addition to the crowbar circuit which protects the RSC from the rotor over-current when the grid fault happens.

For the PMSG wind turbine systems, a braking chopper (BC) with the low cost advantage and the simple control has been employed for the LVRT [12], [13], [14]. However, it is not so easy to improve the power quality at the output of the wind turbine systems since the BC can just dissipate the power with no capability of returning the power to the system. Moreover, the STATCOM has been applied to maintain the wind turbine system connected to the grid during the grid faults [15]. By using this method, the regulation of the voltage is considerably improved in both the transient state and the steady-state. However, the STATCOM can not be used alone without the BC. Another different solution which employs the energy storage system (ESS) can not only offer a ride-through capability but also suppress the output power fluctuation of the wind turbine systems [16]. In this method, in order to reduce the ESS power capacity that it can absorb the full differential power during the grid voltage fault, the generator speed can be increased to store the kinetic energy in the system inertia. However, the ESS power capacity required for the LVRT is still higher than the level of output power fluctuation in the wind turbine systems. So, the designed power capacity of the ESS will be fully utilized only under deep voltage sags for a short time, which occur rarely. Therefore, this ESS system designed for the extreme case is too expensive.

In the PMSG wind turbine system, the generator is connected to the grid through the full-scale back-to-back PWM converters. Normally, DC-link voltage is controlled to be a constant at the grid-side converter, while the machine-side converter controls the active power. For grid voltage faults, the grid-side converter (GSC) in the conventional control method may be out of control. When the grid fault happens, the DC-link voltage is excessively increased due to the continuous operation of WT and generator. However, the overall generated power cannot deliver to the grid fully.

A few researches have been presented that the DC-link voltage control schemes are employed at the machine-side converter instead of the grid-side converter [17], [18]. By increasing the generator speed during the grid voltage sag, the DC-link voltage can be controlled to be constant. However, the response of the DC-link voltage is still not good although a hybrid adaptive PI controller is applied, depending on the relationship between the power and energy [17]. In the proposed method, the MSC controls the DC-link voltage, and the GSC controls the active power for the MPPT.

In some cases, the DC-link voltage control is not regarded as the nonlinear characteristics of the wind power system. By using feedback linearization (FL), a linearized system is obtained and then the DC-link voltage can be designed by the classical linear control theory.

For MPPT, in the conventional optimal torque control method, the torque reference is proportional to the square of the generator speed and the generator torque is controlled to reach its optimal value which corresponds to the maximum power conversion coefficient [19], [20]. Due to the relatively low variation of the generator speed in the large wind turbines, the variation of the generator power is also narrow. The shortcoming of the optimal torque control is the slow response time for wind speed variations.

The aforementioned MPPT methods are based on the steady state characteristics where the effect of the turbine inertia is ignored. Thus, a new method has been proposed for the fast MPPT performance, in which the large inertia effect of the wind turbine was investigated. A proportional controller is added to the torque control to decrease the effect of the moment of inertia of the wind turbines. To verify the effectiveness of the proposed algorithm, the simulation results for the 2-MW PMSG wind turbine system are provided.

This paper is organized as follows. The modeling of the wind turbine systems is described in Section 2. Next, the PMSG control system consisting of conventional method and proposed method for both machine-side converter and grid-side converter is analyzed in Section 3. Then, the simulation results for the PMSG wind turbine system are investigated in Section 4. Finally, the conclusion is presented in Section 5.

2. Modeling of Wind Turbine Systems

2.1. Modeling of Wind Turbines

The output power of WT (P_t) is determined as [20]:

$$P_t = \frac{1}{2}\rho\pi R^2 C_p(\lambda,\beta)V^3, \tag{1}$$

where ρ is the air density [$\mathrm{kg}\cdot\mathrm{m}^{-3}$], R is the radius of blade [m], V is the wind speed [$\mathrm{m}\cdot\mathrm{s}^{-1}$], and $C_p(\lambda,\beta)$ is the power conversion coefficient which is a function of the tip-speed ratio (TSR) and the pitch angle (β),

in which the TSR is defined as [20]:

$$\lambda = \frac{R\omega_t}{V}. \tag{2}$$

The $C_p(\lambda, \beta)$ is expressed as:

$$C_p(\lambda, \beta) = c_1 \left(c_2 \frac{1}{\Lambda} - c_3\beta - c_4\beta^{c_5} - c_6 \right) exp\left(-c_7 \frac{1}{\Lambda} \right), \tag{3}$$

where

$$\frac{1}{\Lambda} = \frac{1}{\lambda + 0.08\beta} - \frac{0.035}{1 + \beta^3} \tag{4}$$

and $c_1 - c_7$ are the constants [21].

The turbine torque can be expressed as:

$$T_t = \frac{1}{2}\rho\pi R^3 \frac{C_p(\lambda, \beta)}{\lambda} V^2. \tag{5}$$

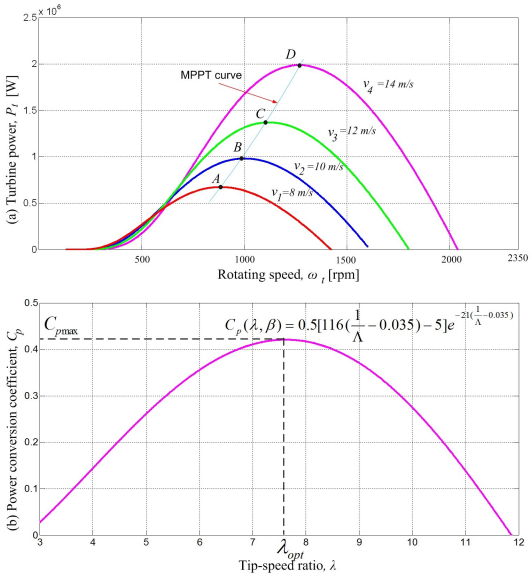

Fig. 1: Wind turbine characteristics: (a) $P_t - \omega_t$ curve, (b) $C_p - \lambda$ curve.

The WT is characterized by $(P_t - \omega_t)$ and $(C_p - \lambda)$ curves as shown in Fig. 1. In Fig. 1(b), the power coefficient, C_{pmax}, has its maximum value at the optimal TSR, λ_{opt}. Thus, to maximize the C_p, the WECS must operate at the λ_{opt}. However, when the wind speed changes, the TSR is out of the optimal value. To keep the optimal TSR, the rotational speed needs to be adjusted by the control system.

2.2. Modeling of PMSG

The stator voltage equations of the PMSG are expressed in the synchronous $d - q$ coordinates as [22], [23], [24]:

$$V_{ds} = R_s I_{ds} + L_s \frac{dI_{ds}}{dt} - \omega_r L_d I_{qs}, \tag{6}$$

$$V_{qs} = R_s I_{qs} + L_s \frac{dI_{qs}}{dt} + \omega_r L_q I_{ds} + \omega_r \lambda_f, \tag{7}$$

where I_{ds} and I_{qs} are d, q-axis stator currents, R_s and L_s are stator resistance and inductance, L_d and L_q are d, q-axis inductance, λ_f is magnet flux, and ω_r is electrical angular speed.

For the generator with surface-mounted permanent magnets, d- and q-axis inductances are the same. Then, the electromagnetic torque T_e is expressed as:

$$T_e = \frac{3}{2}\frac{p}{2}\lambda_f I_{qs}, \tag{8}$$

where p is the number of poles.

The output electrical power can be calculated as:

$$P_g = 1.5(V_{qs} I_{qs} + V_{ds} I_{ds}). \tag{9}$$

2.3. Modeling of Shaft System

The turbine torque with one-mass modeling of wind turbine systems is expressed as [23], [24]:

$$T_t = J_t \frac{d\omega_t}{dt} + T_g + B_t\omega_t, \tag{10}$$

where J_t is the combined inertia of the turbine and generator, B_t is the damping coefficient of turbine, ω_t is the rotor speed of wind turbine, and T_g is the generator torque.

3. PMSG Control System

3.1. Control of Machine-Side Converter for Constant DC Voltage

1) Conventional DC-Link Voltage Control

The control loop of the pulse-width modulation (PWM) converter usually consists of the outer DC-link voltage controller and inner AC input current controller. The IP DC-link voltage controller is preferred since it gives less overshoot than the PI-type [26]. The controller output is given by:

$$I_{qs}^* = [-K_p V_{dc} + K_i \int (V_{dc}^* - V_{dc})dt] + \frac{P_{out}}{1.5V_{qs}}. \tag{11}$$

The last term in Eq. (11) is a feed-forward control component for output power (P_{out}). The power balance of the input and output of the DC-link is expressed as:

$$\frac{C}{2}\frac{dV_{dc}^2}{dt} = P_{in} - P_{out}, \tag{12}$$

where C is the DC-link capacitance, P_{in} is the input power of the PWM inverter, which is obtained from Eq. (9).

For the PMSG, to achieve maximum torque control sensitivity, and improve dynamic machine response, $d-$axis current (I_{ds}) in Eq. (9) is controlled to zero. Thus, Eq. (9), Eq. (11) and Eq. (12) are expressed as:

$$\frac{C}{2}\frac{dV_{dc}^2}{dt} = 1.5V_{qs}[-K_pV_{dc} + K_i\int(V_{dc}^* - V_{dc})dt]. \quad (13)$$

Expanding Taylor series of the DC-link voltage at operating point(V_{dc0}) and neglecting higher-order terms,

$$V_{dc}^2 = V_{dc0}^2 + 2(V_{dc} - V_{dc0}). \quad (14)$$

From Eq. (13) and Eq. (14), the transfer function of the DC-link voltage and its reference can be derived from power balance of the input and output of the DC-link as [26]:

$$\frac{V_{dc}(s)}{V_{dc}^*(s)} = \frac{\frac{1.5V_{qs}K_i}{CV_{dc}^*}}{s^2 + \frac{1.5V_{qs}K_p}{CV_{dc}^*}s + \frac{1.5V_{qs}K_p}{CV_{dc}^*}} = \frac{\omega_n^2}{s^2 + 2\xi\omega_n s + \omega_n^2}, \quad (15)$$

where $V_{qs} = V_{max}$ is the $q-$axis generator output voltage, ω_n is the undamped natural frequency and ξ is the damping ratio. From Eq. (15), the proportional and integral gains are obtained as:

$$K_p = 2\xi\omega_n\frac{CV_{dc}^*}{1.5V_{qs}}, \quad (16)$$

$$K_i = \omega_n^2\frac{CV_{dc}^*}{1.5V_{qs}}. \quad (17)$$

In this research, the controller gains are selected as $K_p = 14.21$ and $K_i = 803.87$ by setting $\xi = 0.707$ and $\omega_n = 80$ [rad/s], which are selected by experience.

2) Nonlinear Modeling

To design the DC-link voltage controller, the dynamic characteristics of wind turbines in the PMSG wind power system are considered. Neglecting the converter loss, the generator power and the DC-link capacitor power can be expressed as:

$$P_g = P_t - J_t\omega_t\frac{d\omega_t}{dt} - B_t\omega_t^2 - P_{g.loss}, \quad (18)$$

$$P_{cap} = CV_{dc}\frac{dV_{dc}}{dt} = P_g - P_{grid}, \quad (19)$$

where P_g is the generator power, P_{grid} is the grid power, $P_{g.loss}$ is the generator loss, P_{cap} is the DC-link capacitor power, V_{dc} is the DC-link voltage, C is the DC-link capacitor.

From Eq. (18) and Eq. (19), a dynamic equation for the PMSG wind turbine system is expressed as:

$$P_{grid} = P_t - J_t\omega_t\frac{d\omega_t}{dt} - B_t\omega_t^2 - P_{g.loss} - CV_{dc}\frac{dV_{dc}}{dt}. \quad (20)$$

A nonlinear relation between V_{dc} and ω_t is shown in Eq. (19). This nonlinear equation can be linearized using a feedback linearization theory, which will be described in the following section.

3) Feedback Linearization

A single-input and single-output nonlinear system is expressed as [27], [28]:

$$\dot{x} = f(x) + g(x)u, \quad (21)$$

$$y = h(x), \quad (22)$$

where x is the state vector, u is the control input, y is the output, f and g are the smooth vector fields, respectively, and h is the smooth scalar function.

The nonlinear equations in Eq. (18) and Eq. (19) are expressed in the form of Eq. (21) as follows:

$$\begin{bmatrix}\dot{V_{dc}}\\ \dot{\omega_t}\end{bmatrix} = \begin{bmatrix}-\frac{P_{grid}}{CV_{dc}}\\ \frac{P_t}{J_t\omega_t} - \frac{B_t\omega_t}{J_t} - \frac{P_{g.loss}}{J_t\omega_t}\end{bmatrix} + \begin{bmatrix}\frac{1}{CV_{dc}}\\ -\frac{1}{J\omega_m}\end{bmatrix}\cdot P_g. \quad (23)$$

In Eq. (23), the DC-link voltage is selected as an output. For the linearization, a relation between input and output should be delivered. So, the output y in Eq. (22) is differentiated as [29]:

$$\dot{y} = \nabla h(f + g\cdot u) = L_fh(x) + L_gh(x)\cdot u, \quad (24)$$

where $L_fh(x)$ and $L_gh(x)$ represent Lie derivatives of $h(x)$ with respect to $f(x)$ and $g(x)$, respectively. The Lie derivative is defined as [29]:

$$L_fh = \nabla hf = \frac{\partial h}{\partial x}\cdot f. \quad (25)$$

If L_fh and L_gh are replaced to $A(x)$ and $E(x)$, the output of the system is obtained as:

$$\dot{y} = A(x) + E(x)u, \quad (26)$$

where

$$A(x) = -\frac{1}{CV_{dc}}P_{grid} \text{ and } E_x = \frac{1}{CV_{dc}}. \quad (27)$$

If a control input u is chosen as:

$$u = E^{-1}(x)[-A(x) + v], \tag{28}$$

where v is the equivalent control input to be specified. The resultant dynamics become linear as:

$$\dot{y} = v. \tag{29}$$

To eliminate the tracking error in the presence of parameter variations, the new control input with an integral control is given by:

$$v = \dot{y}^* - k_1 e - k_2 \int e\, dt, \tag{30}$$

where $e = y - y^*$, y^* is the tracking reference, and k_1 and k_2 are the controller gains.

If the all gains of k_1 and k_2 are positive, the tracking error converges to zero. From Eq. (30), we obtain error dynamics as:

$$\ddot{e} + k_1\dot{e} + k_2 e = 0. \tag{31}$$

By locating the desired poles on the left-half plane, the controller gains are determined and asymptotic tracking control to the reference is achieved [27], [30]. It is assumed that the solution of Eq. (30) is expressed as:

$$s_{1,2} = -\alpha \pm j\beta \ (\alpha > 0,\ \beta > 0). \tag{32}$$

In this work, by selecting the poles at $s_{1,2} = -75 \pm j50$ which are based on experience, the gains can be obtained as $k_1 = 1.5$ and $k_2 = 81.3$.

4) Control of Machine-Side Converter

The operation of the GSC is directly affected by the unbalanced grid voltage, in which the generator power delivered to the grid is restricted. During this grid fault duration, the wind turbine and generator should keep operating as if they do in the normal condition. Thus, the power transferred from the generator side may make an increase in the DC-link voltage. Differently from the conventional control of the AC/DC converter, the DC-link voltage is controlled by the machine-side converter instead of the GSC. The basic principle is that the generator-side converter should try to adjust the generator output power to balance the load power need, such that the dc-link voltage can be maintained.

From Eq. (23) to Eq. (32), the block diagram of the proposed nonlinear DC-link voltage control is partially shown in Fig. 2. Unlikely the conventional method, the generator power reference is produced through the DC-link voltage controller instead of the maximum power point tracking controller. For vector control of a PMSG, the cascaded control structure of the machine-side converter is composed of the outer generator power control loop and the inner current control loop. In order to obtain maximum torque at a minimum current, the $d-$axis reference current component is set to zero and then the $q-$axis current is proportional to the active generator power, which is determined by the DC-link voltage controller.

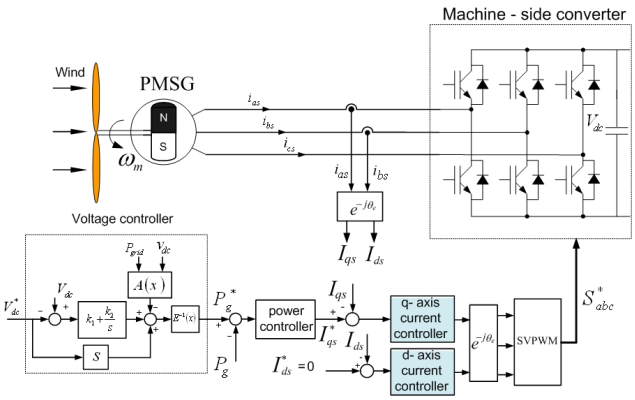

Fig. 2: Control block diagram of the machine-side converter.

3.2. Control of Grid-Side Converter for MPPT

1) Optimal Torque Control

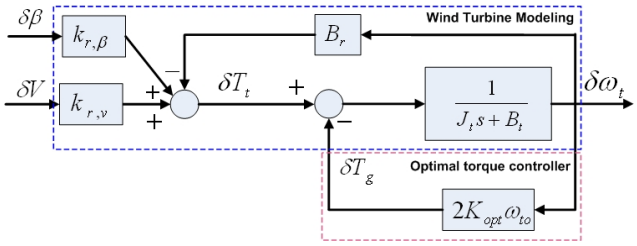

Fig. 3: Wind turbine modeling including the optimal torque control.

For the small signal analysis, applying a small perturbation at the operating point $(\omega_{t0}, \beta_0, V_0)$ to the turbine torque in Eq. (10):

$$\begin{aligned}(T_{to} + \delta T_t) &= J_t \frac{d(\omega_{to} + \delta\omega_t)}{dt} \\ &+ B_t(\omega_{to} + \delta\omega_t) + (T_{go} + \delta T_g).\end{aligned} \tag{33}$$

As mentioned above, the turbine torque is a function of the wind speed, generator speed and pitch angle. Making the partial derivative from Eq. (5), the turbine torque is expressed as [13]:

$$\delta T_t = -B_r \cdot \delta\omega_t + k_{r,\beta} \cdot \delta\beta + k_{r,V} \cdot \delta V, \tag{34}$$

B_r is the intrinsic speed feedback of the turbine, $k_{r,\beta}$ denotes the gain between the pitch angle and the turbine torque, and $k_{r,V}$ is the gain between the wind speed and the turbine torque. From Eq. (33) and Eq. (34), the mechanical torque is rewritten as:

$$J_t \frac{d\delta\omega_t}{dt} + (B_t + B_r)\delta\omega_t = K_{r,\beta}\delta\beta - \delta T_g + K_{r,V}\delta V. \quad (35)$$

The generator torque reference from the turbine speed is expressed as:

$$T_g^* = K_{opt}\omega_t^2, \quad (36)$$

where

$$K_{opt} = \frac{1}{2}\rho A C_{p\,max}\left(\frac{R}{\lambda_{opt}}\right)^3. \quad (37)$$

In the optimal torque control, the torque reference of the PMSG is linearized at the operating point as follows:

$$\begin{aligned} T_g^*(=T_g) &= T_{g0} + \delta T_g \\ &= K_{opt}(\omega_{t0} + \delta\omega_t)^2 \\ &\approx K_{otp}\omega_{t0}^2 + 2K_{opt}\omega_{t0}\delta\omega_t, \end{aligned} \quad (38)$$

where ω_{t0} is the rotor speed at the operating point.

From Eq. (35) and Eq. (38), the transfer function between the turbine torque and the rotor speed which are shown in Fig. 3 is obtained as:

$$G(s) = \frac{\delta\omega_t}{\delta T_t} = \frac{1}{J_t s + B_t + B_r + 2K_{opt}\omega_{t0}}. \quad (39)$$

2) Proposed Torque Control

When the wind speed varies, the dynamic response in the optimal torque control is restricted since the turbine speed determines the torque reference. To improve the performance of the MPPT control in the transient state, the difference between the turbine torque and the generator torque needs to be large so that the system can accelerate or decelerate quickly. In addition, the MPPT control method has to keep the C_p to be at the maximum value at the steady state. To satisfy this requirement, a proportional controller is added to the optimal torque controller. Then, Fig. 3 is modified to Fig. 4. From this model, the generator torque reference is calculated for the MPPT control.

This controller is effective only in the transient state and its effect vanishes in the steady state where the proposed controller has the same characteristics as the optimal torque one described above. With the proportional control loop, the transfer function in Eq. (39) is modified as:

$$G'(s) = \frac{\delta\omega_t}{\delta T_t} = \frac{1}{J_t' s + B_t' + B_r + 2K_{opt}\omega_{t0}}, \quad (40)$$

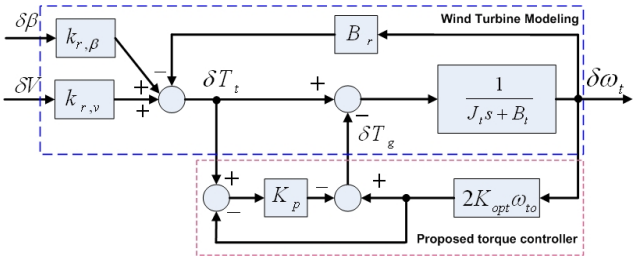

Fig. 4: Wind turbine modeling including the proposed torque control.

where

$$J_t' = \frac{J_t}{1+K_p} \text{ and } B_t' = \frac{B_t}{1+K_p} \quad (41)$$

and K_p is a proportional gain which determines the transient performance of the MPPT control.

It is noticed from Eq. (41) that the inertia moment (J_t') and the damping coefficient (B_t') are effectively decreased by the proportional gain, which makes the dynamic response faster. Thus, a large-inertia wind turbine system can be controlled similarly to a small-scale one under the torque capability of the system. In this research, the gain is empirically selected by a trial and error, which is 1 for the simulation.

Figure 5(a) and Fig. 5(b) show the MPPT control block diagrams for the optimal torque control method and the proposed torque control method, respectively. The torque reference multiplied by the turbine speed (ω_t) obtains the optimal power reference. This MPPT control block diagram can be substituted into the corresponding part in Fig. 4.

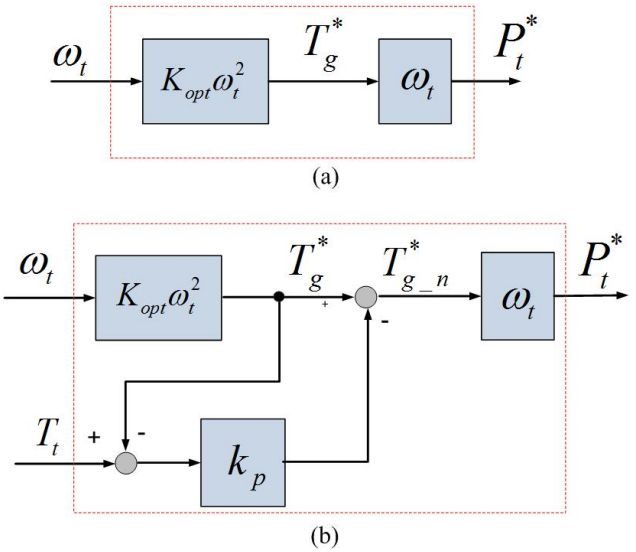

Fig. 5: Block diagram of MPPT control. (a) Optimal torque control. (b) Proposed torque control.

Figure 6 depicts the effect of the inertia on the turbine system according to the rotational speed, at the

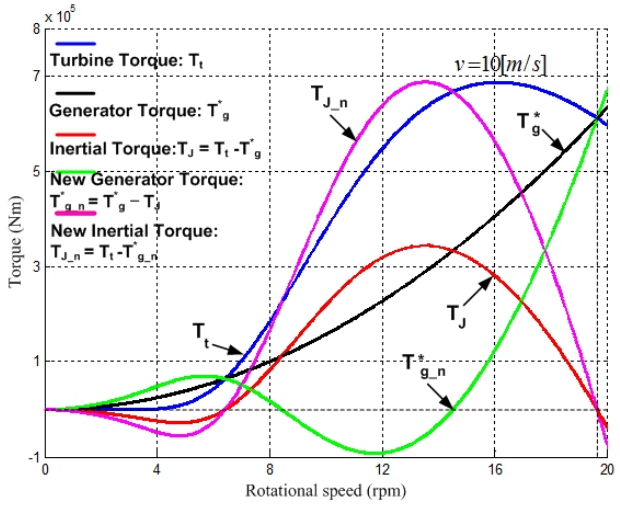

Fig. 6: Inertia effect on the turbine system with and without an added proportional gain.

wind speed of 10 $[\mathrm{m}\cdot\mathrm{s}^{-1}]$, with or without an added proportional control loop, in which the maximum value of the power coefficient, C_{pmax} is 0.41 at the optimal TSR of 7.95.

For the conventional optimal torque control method, an inertial torque (T_j), which leads to acceleration or deceleration of the turbine system, is determined by the difference between the turbine torque and generator torque ($T_t - T_g^*$).

It is noted that the electrical power varies faster than the mechanical one due to the turbine and generator inertia. If an inertia is large, any change of the turbine speed will cause a large variation of the generator power. Then, the kinetic energy is absorbed or released so slowly that the performance of the MPPT becomes slow. Thus, a proportional controller is employed to reduce the effects of the inertia moment and the damping coefficient. With the proposed torque control method, whose block diagram is shown in Fig. 5(b), if the k_p is selected to be 1 as aforementioned, the generator torque reference is decreased to $T^*_{g\_n}$. Then, the inertial torque is increased to T_{J_n} to accelerate the turbine system more quickly. As can be seen from Fig. 6, an inertial torque in the proposed method is larger than that of the optimal torque control method. Thus, the acceleration of the rotor will be faster.

3) Grid Power Reference

As shown in Fig. 5(b), the maximum power of the wind turbine is calculated as:

$$P_t = T^*_{g\_n} \cdot \omega_t. \tag{42}$$

From Eq. (20) and Eq. (42), the grid power reference is given by:

$$P^*_{grid} = T^*_{g\_n} \cdot \omega_t - J_t \frac{\omega_t d\omega_t}{dt} - B_t\omega_t^2 - P_{g.loss} - C\frac{V_{dc}dV_{dc}}{dt}. \tag{43}$$

As can be seen in Eq. (43), the grid power reference (P^*_{grid}) is obtained by applying the MPPT method from the wind turbines.

4) Current Control under Unbalanced Grid Voltage

In unbalanced grid voltage conditions, the positive-sequence voltage component in the stationery reference frame is expressed as [31], [32]:

$$\begin{bmatrix} e^+_{ga} \\ e^+_{gb} \\ e^+_{gc} \end{bmatrix} = \begin{bmatrix} \frac{1}{6}(2e_{ga} - e_{gb} - e_{gc}) - \frac{1}{j2\sqrt{3}}(e_{ga} - e_{gc}) \\ \frac{1}{6}(2e_{gb} - e_{gc} - e_{ga}) - \frac{1}{j2\sqrt{3}}(e_{gc} - e_{ga}) \\ \frac{1}{6}(2e_{gc} - e_{ga} - e_{gb}) - \frac{1}{j2\sqrt{3}}(e_{ga} - e_{gb}) \end{bmatrix}, \tag{44}$$

where e_{ga}, e_{gb}, e_{gc} and e^+_{ga}, e^+_{gb}, e^+_{gc} are the instantaneous grid voltages and the positive-sequence components, respectively. The j in Eq. (44) means the phase shift of 90 degrees, which is obtained by using all-pass filters [32]. The d-axis voltage calculated from the positive-sequence component of the grid voltages is controlled to be zero, from which the reference grid phase angle for control is determined [31].

The apparent power delivered to the grid under unbalanced conditions is expressed in terms of the positive and negative sequence components as [33]:

$$S = 1.5(e^{j\omega t}e^+_{dqs} + e^{-j\omega t}e^-_{dqs}) \cdot (e^{j\omega t}i^+_{dqs} + e^{-j\omega t}i^-_{dqs})^*, \tag{45}$$

where the superscript of "$*$" represents a complex conjugate value, and the superscripts "$+$" and "$-$" are the positive- and negative-sequence components, respectively.

Thus, the apparent power is divided into the active power $p(t)$ and the reactive power $q(t)$ [33].

$$p(t) = P_0 + P_{c2}\cos(2\omega t) + P_{s2}\sin(2\omega t), \tag{46}$$

$$q(t) = Q_0 + Q_{c2}\cos(2\omega t) + Q_{s2}\sin(2\omega t), \tag{47}$$

where

$$
\begin{aligned}
P_0 &= 1.5(E_d^+ I_d^+ + E_q^+ I_q^+ + E_d^- I_d^- + E_q^- I_q^-),\\
P_{c2} &= 1.5(E_d^+ I_d^- + E_q^+ I_q^- + E_d^- I_d^+ + E_q^- I_q^+),\\
P_{s2} &= 1.5(E_d^+ I_q^- - E_q^+ I_d^- - E_d^- I_q^+ + E_q^- I_d^+),\\
Q_0 &= 1.5(-E_d^+ I_q^+ + E_q^+ I_d^+ - E_d^- I_q^- + E_q^- I_d^-),\\
Q_{c2} &= 1.5(-E_d^+ I_q^- + E_q^+ I_d^- - E_d^- I_q^+ + E_q^- I_d^+),\\
Q_{s2} &= 1.5(E_d^+ I_d^- + E_q^+ I_q^- - E_d^- I_d^+ - E_q^- I_q^+).
\end{aligned}
$$

From Eq. (46) and Eq. (47), the power (P_0, Q_0, P_{s2}, P_{c2}) can be represented in a matrix form as:

$$
\begin{bmatrix} P_0 \\ Q_0 \\ P_{s2} \\ P_{c2} \end{bmatrix} = \begin{bmatrix} E_d^+ & E_q^+ & E_d^- & E_q^- \\ E_q^+ & -E_d^+ & E_q^- & -E_d^- \\ E_q^- & -E_d^- & -E_q^+ & E_d^+ \\ E_d^- & E_q^- & E_d^+ & E_q^+ \end{bmatrix} \begin{bmatrix} I_d^+ \\ I_q^+ \\ I_d^- \\ I_q^- \end{bmatrix}. \quad (48)
$$

The second-order components of power (P_{c2}, P_{s2}) due to the unbalanced grid voltage fluctuates not only the DC-link capacitor power but also the real power delivered to the grid. These two components are controlled to zero to eliminate the power fluctuations. The real power reference (P_0^*) is obtained in Eq. (43). The reactive power reference (Q_0^*) can be determined from unity power factor operation or the grid requirements. Therefore, the positive- and negative-sequence components of the current references are expressed as:

$$
\begin{bmatrix} I_d^{+*} \\ I_q^{+*} \\ I_d^{-*} \\ I_q^{-*} \end{bmatrix} = \begin{bmatrix} E_d^+ & E_q^+ & E_d^- & E_q^- \\ E_q^+ & -E_d^+ & E_q^- & -E_d^- \\ E_q^- & -E_d^- & -E_q^+ & E_d^+ \\ E_d^- & E_q^- & E_d^+ & E_q^+ \end{bmatrix} \begin{bmatrix} P_{grid}^* \\ Q_0^* \\ 0 \\ 0 \end{bmatrix}. \quad (49)
$$

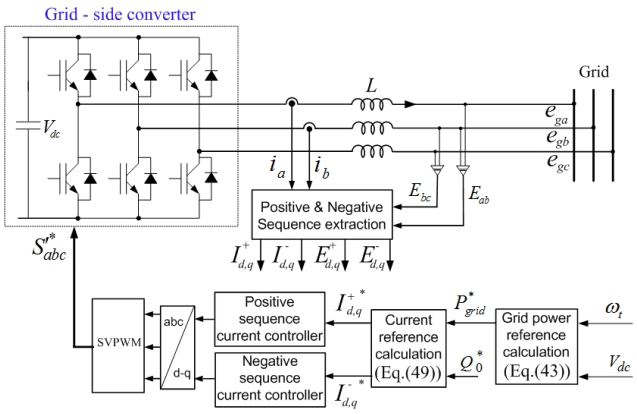

Fig. 7: Control block diagram of the grid-side converter.

The control block diagram of the GSC consisting of the dual current controller for positive- and negative-sequence components is shown in Fig. 7 [33].

4. Simulation Studies

To verify the effectiveness of the proposed method, the simulation has been carried out using the PSIM software for a 2-MW PMSG wind turbine. The parameters of the wind turbine and generator are listed in Tab. 1 and Tab. 2, respectively. The DC-link voltage is controlled at 1,300 V, the DC-link capacitance is 0.1 F, the switching frequency is 2 kHz, and the grid voltage is 690 V_{rms}/60 Hz.

Tab. 1: Parameters of wind turbine.

Rated power	2 MW
Blade radius	45 m
Air density	1.225 kg· m^{-3}
Max. power conv. coefficient	0.411
Cut-in speed	3 m/s
Cut-out speed	25 m/s
Rated wind speed	10.6 m/s
Blade inertia	$6.3 \cdot 10^6$ kg $\cdot$ m^2

Tab. 2: Parameters of 2 MW PMSG.

Rated power	2 MW
Grid voltage	690 V
Stator voltage/frequency	690 V/60 Hz
Stator resistance	0.008556 Ω
d-axis inductance	0.00359 H
q-axis inductance	0.00359 H

4.1. Proposed MPPT Control

Figure 8 and Fig. 9 show the dynamic responses of the optimal torque control (conventional control method) and the proposed torque control methods, respectively, when the wind speed changes from 6 m $\cdot$ s^{-1} to 8 m $\cdot$ s^{-1} at 20 s and back to 6 m $\cdot$ s^{-1} at 50 s. For the easy investigation, the grid is assumed to be normal. Also, the damping coefficient is neglected in the simulation.

Figure 8(b) shows the power conversion coefficient, C_P, which is recovered to C_{Pmax} in 1.5 s after the sudden drop at 20 s. Meanwhile, it takes just 0.6 s for the proposed torque control method. Compared with the optimal torque control method, the C_P in the proposed method gives the faster response during the step-wise change of the wind speed. Also, the actual turbine power P_t as shown in Fig. 8(c) reaches steady state after 1.5 sec, while it takes just 0.5 sec for the proposed torque control method (Fig. 9(c)).

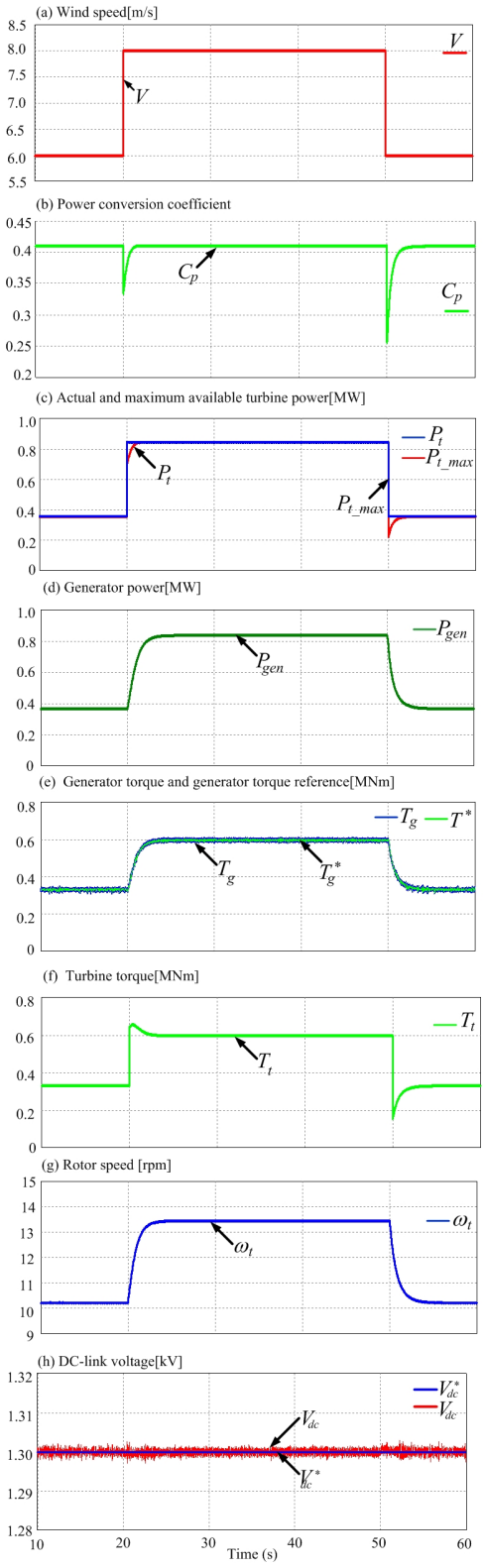

Fig. 8: Responses of optimal torque control in step-wise wind speed variation: (a) wind speed, (b) power conversion coefficient, (c) actual and maximum available turbine power, (d) generator power, (e) generator torque and generator torque reference, (f) turbine torque, (g) rotor speed, (h) DC-link voltage.

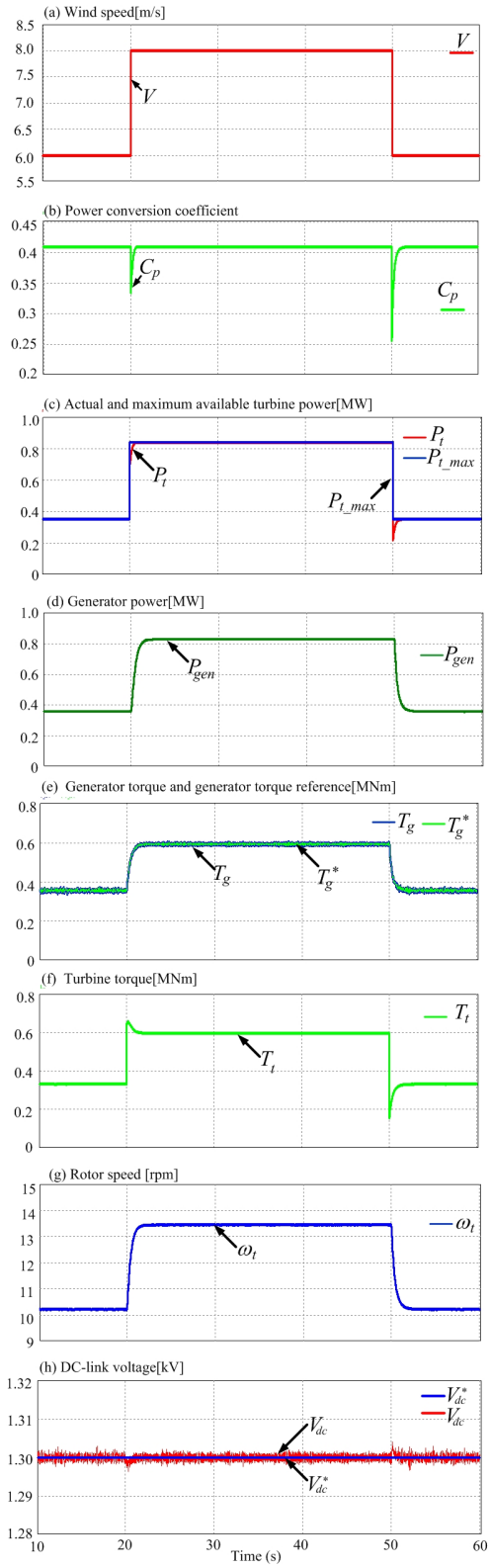

Fig. 9: Responses of proposed torque control in stepwise wind speed variation: (a) wind speed, (b) power conversion coefficient, (c) stator active power, (d) turbine torque, generator torque and generator torque reference, (e) actual and maximum available turbine power, (f) generator speed.

As can be seen in Fig. 8(d), the generated active power is also varied, and then, reaches the steady state after 4.4 sec. However, in the proposed torque control method as shown in Fig. 9(d), this value gives the faster performance than that of the conventional control method.

The actual generator torque, generator torque reference, and the turbine torque are illustrated Fig. 8(e) and Fig. 8(f), respectively. With the conventional method, the generator torque follows its reference value and reaches the steady state after 4.5 s. But, with the proposed method, the actual generator torque, the generator torque reference and turbine torque as shown in Fig. 9(e) and Fig. 9(f), respectively, becomes better when compared with the conventional one. With the same pattern of the wind speed, the generator speed in both cases is increased. However, as shown in Fig. 9(g), the generator speed in the proposed method accelerates faster than it does in the optimal torque control one, as illustrated in Fig. 8(g). As a result, more turbine power can be captured. The proposed torque control method provides better performance than the optimal torque control one in transient state due to the proportional controller.

By applying the feedback linearization at the MSC, the generator is controlled to keep the DC-link voltage to follows its reference well and is maintained within variation of less than 1 %, as illustrated in Fig. 8 and Fig. 9(h).

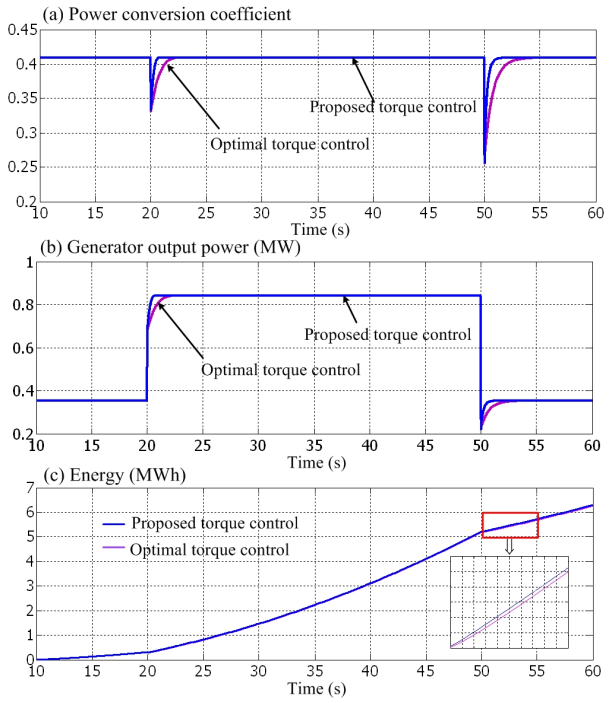

Fig. 10: Comparison of performance responses between optimal torque control method and proposed torque control method: (a) power conversion coefficient, (b) generator output power, (c) Energy.

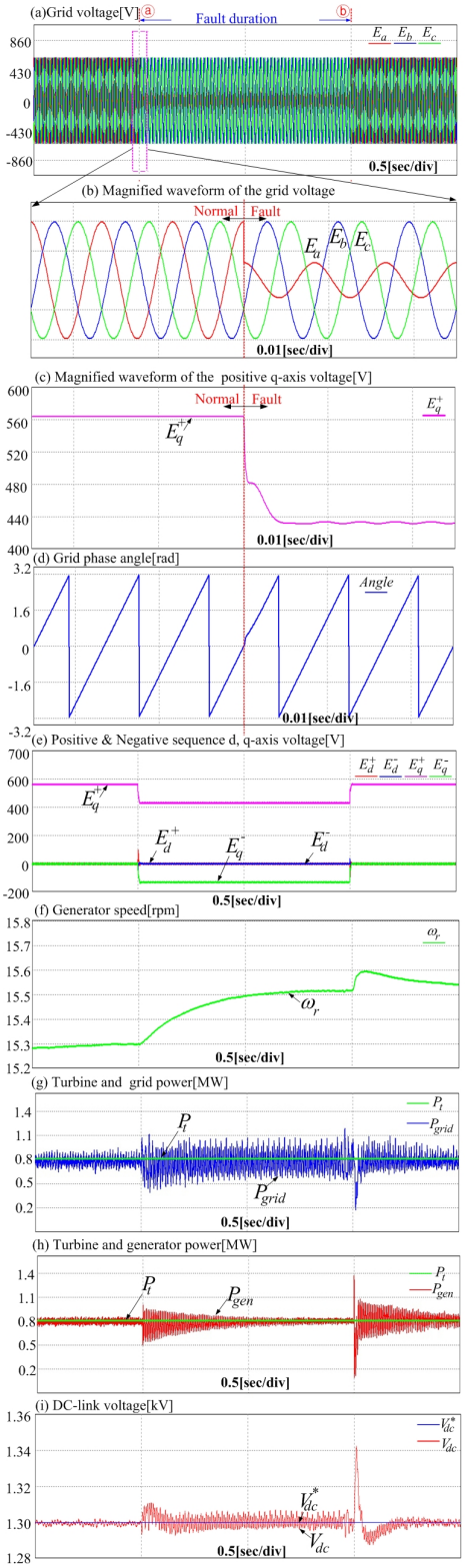

Fig. 11: Wind power generation performance for grid phase-A voltage sag: (a) grid voltage, (b) magnified waveform of the grid voltage, (c) magnified waveform of positive q-axis voltage, (d) grid phase angle, (e) positive and negative sequence $d-q$ axis voltage, (f) generator speed, (g) turbine and grid power, (h) turbine and generator power, (i) DC-link voltage.

Figure 10 shows the comparison of the responses of the power conversion coefficient, generator output power and energy, with the same wind profile as Fig. 8(a), for both optimal torque control and proposed torque control methods. As can be seen, the MPPT using the proposed torque control method gives good performance. It is evaluated that the average power conversion coefficient with the proposed torque control method is 0.63 % higher than that of using the optimal torque control one. Also, with the proposed method, the energy production is also 0.43 % larger than that of with the optimal torque control method. Of course, the energy production will depend on the wind speed profile and the proportional gain, etc.

4.2. DC-Link Voltage Control

Figure 11 shows the system performance for a grid unbalanced voltage sag, in which the wind speed is assumed to be constant ($8\ \mathrm{m}\cdot\mathrm{s}^{-1}$) for easy examination. The fault condition is 70 % sag in the grid A-phase voltage for 1 sec (60 cycles), which is between the point "a" to "b" as shown in Fig. 11(a). Figure 11(b) and Fig. 11(c) shows the magnified grid voltages and the magnified grid positive q-axis, respectively, for 6 cycles just before and after fault. Also, the grid phase angle for control using the phase locked-loop algorithm under unbalance conditions [31], [32] is illustrated in Fig. 11(d). Fig. 11(e) shows the positive- and negative-sequence $d-q$ axis voltages. Due to the grid unbalanced voltage sag, the positive-sequence q-axis voltage is reduced and the negative-sequence $d-q$ voltage components appear. During the grid fault duration, the generator speed is increased to keep the DC-link voltage constant as shown in Fig. 11(f). Also, the grid, generator and turbine powers are illustrated in Fig. 11(g) and Fig. 11(h). Figure 11(i) shows the DC-link voltage response, where the maximum voltage variation at the transient state is about 3.1 %.

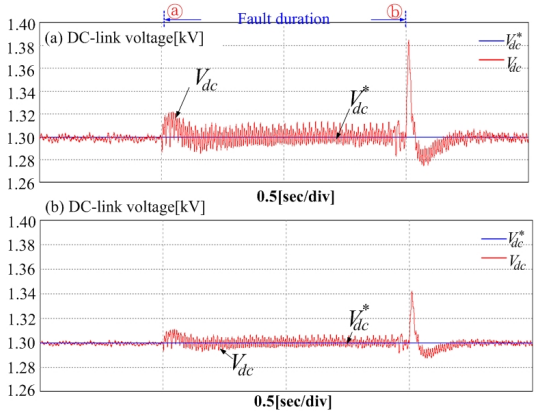

Fig. 12: Performance of DC-link voltage control with: (a) PI control, (b) FL control.

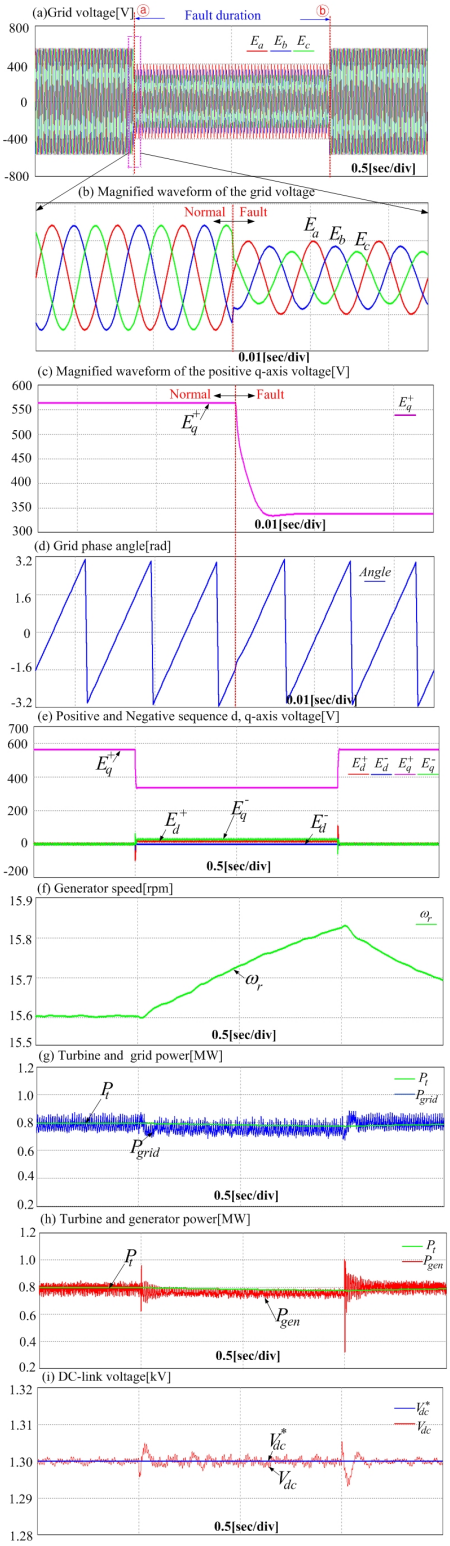

Fig. 13: Wind power generation performance for three-phase unbalance voltage drops (30%-phase A, 40%-phase B, 50%-phase C): (a) Grid voltage, (b) magnified waveform of the grid voltage, (c) magnified waveform of positive q-axis voltage, (d) grid phase angle, (e) positive and negative sequence $d-q$ axis voltage, (f) generator speed, (g) turbine and grid power, (h) turbine and generator, (i) DC-link voltage.

Figure 12 shows the DC-link voltage responses for both the PI control and feedback linearization control in the same grid fault condition (70 % sag in the grid A-phase). The proposed method gives faster transient response and lower overshoot (3.1 % of the maximum DC-link voltage variation using the feedback linearization control is compared with 6.9 % of its variation using the PI control).

Figure 13 shows the performance of the system for grid unbalanced voltage sags which are 30 %, 40 %, and 50 % for phase-A, B-phase, and C-phase voltages, respectively, for 1 second, which is between the point "a" to "b" as shown in Fig. 13(a). Figure 13(b) and Fig. 13(c) shows the magnified grid voltages and the magnified grid positive q-axis, respectively, for 6 cycles just before and after fault. Also, the reference grid phase angle using the phase locked-loop algorithm during transient states as well as unbalance conditions [31], [32] is shown in Fig. 13(d). Figure 13(e) illustrates the positive- and negative-sequence $d-q$ axis voltages, in which the positive-sequence q-axis voltage is reduced during the grid fault duration. Figure 13(f) shows the generator speed which is increased to maintain the DC-link voltage to follow its reference. The turbine, generator and grid powers are illustrated in Fig. 13(g) and Fig. 13(h). Figure 13(i) shows the DC-link voltage response, in which its voltage variation is controlled within 0.38 %.

Figure 14 shows the comparison of the responses of the DC-link voltage for both the conventional PI controllers and the feedback linearization method in the same grid fault condition (30 %, 40 %, and 50 % sags for phase-A, B-phase, and C-phase voltages, respectively). It is apparent that the proposed method gives faster response and lower overshoot than the conventional PI (0.38 % of the variation of the DC-link voltage using the feedback linearization control is compared with 1.15 % of its variation using the PI control).

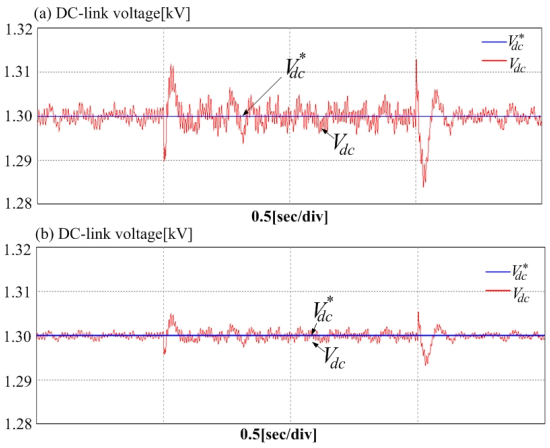

Fig. 14: Performance of DC-link voltage control with: (a) PI control, (b) FL control.

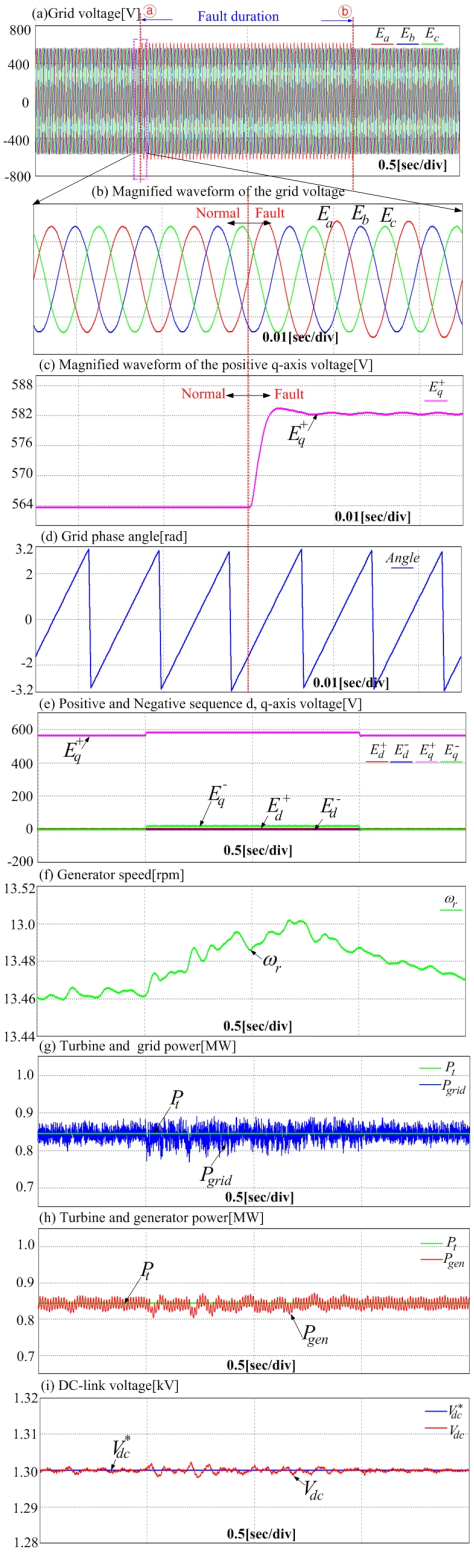

Fig. 15: Wind power generation performance for grid-phase A voltage swell: (a) grid voltage, (b) magnified waveform of the grid voltage, (c) magnified waveform of positive q-axis voltage, (d) grid phase angle, (e) positive and negative sequence $d-q$ axis voltage, (f) generator speed, (g) turbine and grid power, (h) turbine and generator, (i) DC-link voltage.

Figure 15 shows the performance of the system for a grid unbalanced voltage swell. The fault condition is 10 % swell in the grid A-phase voltage for 1 sec (60 cycles), which is between the point "a" to "b" as shown in Fig. 15(a). The magnified grid voltages and the magnified grid positive q-axis for 6 cycles just before and after fault are shown in Fig. 15(b) and Fig. 15(c), respectively. In addition, the grid phase angle for control under fault conditions is illustrated in Fig. 15(d). Figure 15(e) shows the positive- and negative-sequence $d-q$ axis voltages. The positive-sequence q-axis voltage is increased and the negative-sequence $d-q$ voltage components occur due to the grid unbalanced voltage swell. As shown in Fig. 15(f), the generator speed is increased to maintain the DC-link voltage constant during the fault duration. Also, the grid, generator and turbine powers are illustrated in Fig. 15(g) and Fig. 15(h). Figure 15(i) shows the response of the DC-link voltage, in which the variation of the maximum voltage at the transient state is about 0.385 %.

Figure 16 shows the responses of the DC-link voltage for both the conventional PI control and feedback linearization control methods under the same grid fault condition (10 % swell in the grid A-phase). The proposed method gives faster transient response and lower overshoot, compared with the PI control one.

5. Conclusions

This paper proposes the control strategies of the back-to-back PWM converters in PMSG wind power system, for the grid voltage faults and for the MPPT. At the grid fault, a method is based on the DC-link voltage control at the machine-side converter, using feedback linearization technique. The MPPT strategy, where a proportional controller is added to the torque controller to improve the dynamic performance of the MPPT control, is developed to control the grid power at the grid-side converter. The validity of the control algorithm has been verified by simulation results for 2 MW PMSG wind power system.

Acknowledgment

This research is supported by Sai Gon University, Van Hien University, Ho Chi Minh city, Vietnam and supported in part by the National Key Lab of Digital Control and System Engineering-University of Technology-Vietnam National University Ho Chi Minh city.

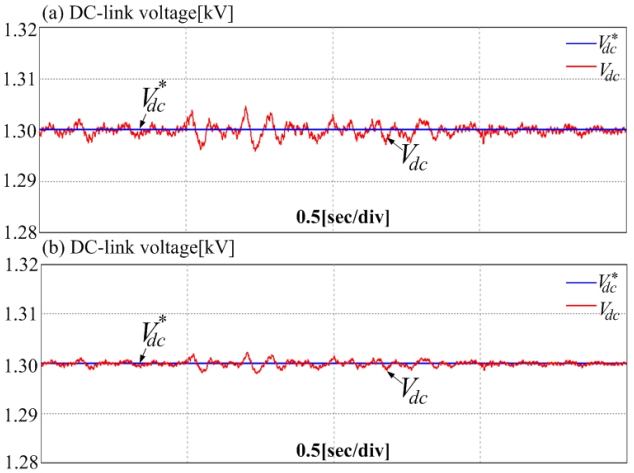

Fig. 16: Performance of DC-link voltage control with: (a) PI control, (b) FL control.

References

[1] CHINCHILLA, M., S. ARNALTES and J. C. BURGOS. Control of permanent-magnet generators applied to variable-speed wind-energy systems connected to the grid. *IEEE Transactions on Energy Conversion*. 2006, vol. 21, iss. 1, pp. 130–135. ISSN 0885-8969. DOI: 10.1109/TEC.2005.853735.

[2] POLINDER, H., F. F. A VAN DER PIJL and P. TAVNER. Comparison of direct-drive and geared generator concepts for wind turbines. *IEEE Transactions on Energy Conversion*. 2006, vol. 21, iss. 3, pp. 725–733. ISSN 0885-8969. DOI: 10.1109/TEC.2006.875476.

[3] IOV, F., A. D. HANSEN, P. SORENSEN and N. A. CUTULULIS. Mapping of grid faults and grid codes. *Technical Report Riso-R-1617(EN)*. Roskilde, Riso National Laboratory, Technical University of Denmark, 2007. ISBN 978-87-550-3622-2.

[4] SANITER, C. and J. JANNING. Test bench for grid code simulations for Multi-MW wind turbines, design and control. *IEEE Transactions on Power Electronics*. 2008, vol. 23, iss. 4, pp. 1707–1715. ISSN 0885-8993. DOI: 10.1109/TPEL.2008.925425.

[5] JEON, J.-H., S.-K. KIM, C.-H. CHO, J.-B. AHN and E.-S. KIM. Development of simulator system for micro-grids with renewable energy sources. *Journal of Electrical Engineering and Technology*. 2006, vol. 1, iss. 4, pp. 409–413. ISSN 2093-7423. DOI: 10.5370/JEET.2006.1.4.409.

[6] POLLIN, R., H. G. PELTIER and H. SCHARBER. Green recovery: A new pro-

gram to create good jobs and start building a low-carbon economy. In: *PERI Political Economy Research Institute* University of Massachusetts, 2007. [online] Available at: http://www.peri.umass.edu/fileadmin/pdf/other_publication_types/peri_report.pdf.

[7] LIMA, F. K. A., A. LUNA, P. RODRIGUEZ, E. H. WATANABE and F. BLAABJERG. Rotor voltage dynamics in the doubly fed induction generator during grid faults. *IEEE Transactions on Power Electronics*. 2010, vol. 25, iss. 1, pp. 118–130. ISSN 0885-8993. DOI: 10.1109/TPEL.2009.2025651.

[8] MEEGAHAPOLA, L. G., T. LITTLER and D. FLYNN. Decoupled-DFIG fault ride-through strategy for enhanced stability performance during grid faults. *IEEE Transactions on Sustainable Energy*. 2010, vol. 25, iss. 1, pp. 152–162. ISSN 1949-3029. DOI: 10.1109/TSTE.2010.2058133.

[9] SONG, Q. and W. LIU. Control of a cascade STATCOM with star configuration under unbalanced conditions. *IEEE Transactions on Power Electronics*. 2009, vol. 24, iss. 1, pp. 45–58. ISSN 0885-8993. DOI: 10.1109/TPEL.2008.2009172.

[10] ZHANG, W. H., S.-J. LEE and M.-S. CHOI. Setting considerations of distance relay for transmission line with STATCOM. *Journal of Electrical Engineering and Technology*. 2010, vol. 5, iss. 4, pp. 522–529. ISSN 2093-7423. DOI: 10.5370/JEET.2010.5.4.522.

[11] PIROUZY, H. M. and M. T. BINA. Modular multilevel converter based STATCOM topology suitable for medium-voltage unbalanced systems. *Journal of Power Electronics*. 2010, vol. 10, iss. 5, pp. 572–578. ISSN 1598-2092. DOI: 10.6113/JPE.2010.10.5.572.

[12] BRANDO, G., A. COCCIA and R. RIZZO. Control method of a braking chopper to reduce voltage unbalance in a 3-level chopper. In: *Proc. IEEE International Conference on Industrial Technology*. Hammamet: IEEE, 2004, pp. 975–978. ISBN 0-7803-8662-0. DOI: 10.1109/ICIT.2004.1490208.

[13] CONROY, J. F. and R. WATSON. Low-voltage ride-through of a full converter wind turbine with permanent magnet generator. *IET Renewable Power Generation*. 2007, vol. 1, iss. 3, pp. 182–189. ISSN 1752-1424. DOI: 10.1049/iet-rpg:20070033.

[14] LI, W., C. ABBEY and G. JOOS. Control and performance of wind turbine generators based on permanent magnet synchronous machines feeding a diode rectifier. In: *Proc. IEEE Power Electronics Specialists Conference*. Jeju: IEEE 2006, pp. 1–6. ISBN 0-7803-9716-9. DOI: 10.1109/PESC.2006.1711746.

[15] SINGH, B., R. SAHA, A. CHANDRA and K. AL-HADDA. Static synchronous compensators (STATCOM): a review. *IET Power Electronics*. 2009, vol. 2, iss. 4, pp. 297–324. ISSN 1755-4535. DOI: 10.1049/iet-pel.2008.0034.

[16] NGUYEN, T. H. and D.-C. LEE. Ride-through technique for PMSG wind turbines using energy storage systems. *Journal of Power Electronics*. 2010, vol. 10, iss. 6, pp. 297–324. ISSN 1598-2092. DOI: 10.6113/JPE.2010.10.6.733.

[17] YUAN, X., F. WANG, D. BOROYEVICH, Y. LI and R. BURGOS. DC-link voltage control of a full power converter for wind generator operating in weak-grid systems. *IEEE Transactions on Power Electronics*. 2009, vol. 24, iss. 9, pp. 2178–2192. ISSN 0885-8993. DOI: 10.1109/TPEL.2009.2022082.

[18] HANSEN, A. D. and G. MICHALKE. Multipole permanent magnet synchronous generator wind turbines' grid support capability in uninterrupted operation during grid faults. *IET Renewable Power Generation*. 2009, vol. 3, iss. 3, pp. 333–348. ISSN 1752-1416. DOI: 10.1049/iet-rpg.2008.0055.

[19] MORIMOTO, S., H. NAKAYAMA, M. SANADA and Y. TAKEDA. Sensorless output maximization control for variable-speed wind generation system using IPMSG. *IEEE Transactions on Industry Applications*. 2005, vol. 41, iss. 1, pp. 60–67. ISSN 0093-9994. DOI: 10.1109/TIA.2004.841159.

[20] AKHMATOV, V. *Induction generators for wind power*. Essex: Multi-Science Publishing Company, 2005. ISBN 978-0906522400.

[21] LUBOSNY, Z. *Wind turbine operation in electric power system*. New York: Springer-Verlag Berlin Heidelberg, 2003. ISBN 978-3-540-40340-1.

[22] NGUYEN, T. H., S.-H. JANG, H.-G. PARK and D.-C. LEE. Sensorless control of PM synchronous generators for micro wind turbines. In: *Proc. IEEE Power and Energy Conference*. Johor Bahru: IEEE, 2008, pp. 936–941. ISBN 978-1-4244-2405-4. DOI: 10.1109/PECON.2008.4762607.

[23] DAI, J., D. XU, B. WU and N. R. ZARGARI. Unified DC-link current control for low-voltage ride-through in current-source-converter-based wind energy conversion systems. *IEEE*

Transactions on Power Electronics. 2011, vol. 26, iss. 1, pp. 288–297. ISSN 0885-8993. DOI: 10.1109/TPEL.2010.2059377.

[24] BIANCHI, F. D., H. D. BATTISTA and R. J. MANTZ. *Wind turbine control systems*. London: Springer-Verlang, 2007. ISBN 978-1-84628-492-2. DOI: 10.1007/1-84628-493-7.

[25] VAN, T. L. *Power quality control of variable-speed wind turbines systems*. Gyeongsan, Korea: Yeungnam University, 2012. Ph.D. thesis.

[26] SUL, S. *Control of electric machine drive system*. New York: Wiley-IEEE Press, 2011. ISBN 9780470876541.

[27] LEE, D.-C., G.-M. LEE and K.-D. LEE. DC-bus voltage control of three-phase ac/dc PWM converters using feedback linearization. *IEEE Transactions on Industry Applications*. 2000, vol. 36, iss. 3, pp. 826–833. ISSN 0093-9994. DOI: 10.1109/28.845058.

[28] DELFINO, F., F. PAMPARARO, R. PROCOPIO and M. ROSSI. A feedback linearization control scheme for the integration of wind energy conversion systems into distribution grids. *IEEE Systems Journal*. 2012, vol. 6, iss. 1, pp. 85–93. ISSN 1932-8184. DOI: 10.1109/JSYST.2011.2163002.

[29] SLOTINE, J.-J. E. and W. LI. *Applied nonlinear control*. Englewood Cliffs, NJ: Prentice-Hall, 1991. ISBN 978-0130408907.

[30] CHEN, C.-T. *Linear system theory and design*. Oxford: Oxford University Press, 1999. ISBN 978-0199959570.

[31] IBRAHIM, A. O., T. H. NGUYEN, D.-C. LEE and S.-C. KIM. A fault ride-through technique of DFIG wind turbine systems using dynamic voltage restorers. *IEEE Transactions on Energy Conversion*. 2011, vol. 26, iss. 3, pp. 871–882. ISSN 0885-8969. DOI: 10.1109/TEC.2011.2158102.

[32] LEE, G.-M., D.-C. LEE and J.-K. SEOK. Control of series active power filters compensating for source voltage unbalance and current harmonics. *IEEE Transactions on Industrial Electronics*. 2004, vol. 51, iss. 1, pp. 132–139. ISSN 0278-0046. DOI: 10.1109/TIE.2003.822040.

[33] SONG, H.-S. and K. NAM. Dual current control scheme for PWM converter under unbalanced input voltage conditions. *IEEE Transactions on Industrial Electronics*. 1999, vol. 46, iss. 5, pp. 953–959. ISSN 0278-0046. DOI: 10.1109/41.793344.

About Authors

Tan Luong VAN was born in Vietnam. He received the B.Sc. and M.Sc. degrees in electrical engineering from Ho Chi Minh City University of Technology, Ho Chi Minh city, Vietnam, in 2003 and 2005, respectively, and Ph.D. degree in electrical engineering from Yeungnam University, Gyeongsan, South Korea in 2013. His research interests include power converters, machine drives, wind power generation, power quality and power system.

Thanh Dung NGUYEN born in Vietnam in 1979. He received Engineer degree in program Electrical and electronic engineering from Ho Chi Minh City University of Technology and Education, Vietnam, in 2002, Master degree of Science in Electrical and electronic engineering, University of Transport and Communications, Vietnam, in 2007, and Ph.D. degree in Technical Cybernetics and Informatics from Tomas Bata University in Zlin in 2012. His research interests include secure encryption, optimization, chaos synchronization, and wind power generation system.

Thanh Trang TRAN was born in Vietnam in 1979. He received the B.Sc. and M.Sc. degrees in electrical –electronics engineering from Ho Chi Minh city University of Technology, National University in Ho Chi Minh city, Vietnam, in 2001 and 2004, respectively, and the Ph.D. degree in display engineering from Yeungnam University, South Korea in 2012. His research interests include modeling and simulation of micro-nano electron devices, display engineering, photovoltaic systems, and renewable energy.

Huy Dung NGUYEN was born in Vietnam. He received B.Sc. degree in electrical engineering from Ho Chi Minh City University of Technology and Education, Vietnam, in 1993. His research interests include power converters and renewable energy.